Interface dynamics and the motion of complex singularities

Wei-shen Dai, Leo P. Kadanoff, and Su-min Zhou
The James Franck Institute, The University of Chicago, 5640 South Ellis Avenue, Chicago, Illinois 60637
(Received 25 January 1991)

The motion of the interface between two fluids in a quasi-two-dimensional geometry is studied via simulations. We consider the case in which a zero-viscosity fluid displaces one with finite viscosity and compare the interfaces that arise with zero surface tension with those that occur when the surface tension is not zero. The interface dynamics can be analyzed in terms of a complex analytic function that maps the unit circle into the interface between the fluids. The physical region of the domain is the exterior of the circle, which then maps into the region occupied by the more viscous fluid. In this physical region, the mapping is analytic and its derivative is never zero. This paper focuses upon the determination of the nature of the interface and the positions of the singularities of the derivative of the mapping function g. Two kinds of initial conditions are considered: case A, in which the singularities closest to the unit circle are poles; and case B, in which the $t=0$ interface is described by a function g with only zeros inside the unit circle. In either case, different behaviors are found for relatively smaller and larger surface tensions. In case A, when the surface tension is relatively small, the problem is qualitatively similar with and without surface tension: the singularities move outward and asymptotically approach the unit circle. For relatively large surface tension, the singularities, still polelike, move towards the center of the unit circle instead. In case B, for zero surface tension, the zeros move outward and hit the unit circle after a finite time, whereupon the solution breaks down. For finite but relatively small surface tension, each initial zero disappears and is replaced by a pair of polelike excitations that seem to approach the unit circle asymptotically, while for a relatively large surface tension, each initial zero is replaced by a polelike singularity that then moves towards the unit circle.

I. INTRODUCTION

Bubble growth in a Hele-Shaw cell has drawn much attention recently. Here, two closely spaced glass plates contain two fluids. For this idealized case, one fluid is viscous and incompressible, while the other has zero viscosity. The latter fluid is a bubble in an infinite sea composed of the more viscous fluid. The area of zero-viscosity fluid grows at a steady rate. The interface separating the two fluids is described by a surface tension. This and similar systems, for example, a channel flow geometry, have been studied experimentally, and various growth features have been observed.[1] For some initial conditions, the zero-surface-tension case can be solved analytically.[2–5] These solutions show that for a large range of initial conditions, the interface will develop cusps after a finite time interval. After this critical time, the analysis is not meaningful.

Starting with the work of Saffman and Taylor,[6] there has been considerable discussion of the effect of the surface tension upon the interface motion in a Hele-Shaw cell. Work on this problem has shown that the surface tension is a singular perturbation, so that the solutions with and without surface tension may be qualitatively different.[7] Since the bubble-growth problem is the simplest one in this general class, the question of whether the presence of a small surface tension will qualitatively change the solution is of great interest.

In this paper, we shall first give a mathematical formulation of the bubble-growth problem using a method proposed by Shraiman and Bensimon[8] and Tanveer.[9] After a brief review of the results for the zero-surface-tension case, we shall report our simulation results for the growth of a bubble with nonzero surface tension. We shall show both the shape of the bubbles and the motion of the singularities with surface tension in comparison with those without surface tension. The computational methodology will be described in the Appendix.

II. MATHEMATICAL FORMULATION

The system has two kinds of fluids. They are confined between two parallel glass plates that are kept very close to each other (see Fig. 1). The interface between the two fluids is bubble shaped. The fluid inside the bubble (fluid 1) has a negligible viscosity and is kept at a constant pressure. The fluid outside the bubble (fluid 2) has a larger viscosity and is incompressible.

For the fluid outside the bubble, we can use Darcy's law:

$$\mathbf{v}=-\frac{b^2}{12\mu}\nabla p \ , \tag{1}$$

where $\mathbf{v}$, p, and μ are the velocity, pressure, and viscosity of fluid 2, and b is the spacing between the two plates. From the condition of incompressibility, we have $\nabla\cdot\mathbf{v}=0$. Therefore, the field satisfies the Laplace equation

$$\nabla^2 p=0 \ . \tag{2}$$

The pressure is constant inside the bubble and has a jump

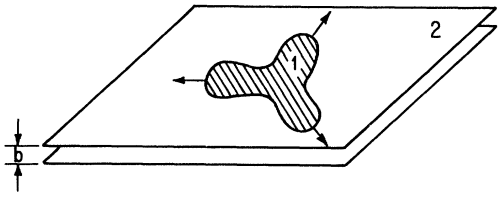

FIG. 1. The Hele-Shaw cell. Fluid 1 and fluid 2 are confined between two plates of distance b. A bubble containing fluid 1 with negligible viscosity grows into fluid 2 with larger viscosity.

at the interface, which is equal to the surface tension τ times the local curvature κ. Since the constant added to the pressure has no dynamical effects, we can write as our boundary conditions

$$p|_{\text{interface}}=\tau\kappa \ . \tag{3}$$

At infinity,

$$p\rightarrow\frac{1}{2\pi}\frac{dS}{dt}\ln r \ , \tag{4}$$

where r is the distance from the injection point.

The boundary condition (3) is not always a fully correct description of the situation in real, three-dimensional fluid cells.[10] In this paper we nonetheless use Eq. (3), in part because it provides an interesting mathematical problem.

A hodographic method is used to solve the equations (see, for example, Refs. 2, 5, and 8). A conformal mapping $f(\omega,t)$ is used to map the unit circle in the ω plane onto the interface in the z plane and the exterior of the unit circle into the exterior of the bubble (see Fig. 2). So in the ω plane, the outside of the unit circle, $|\omega|\geq 1$, corresponds to the physical domain, and the inside of the unit circle $|\omega|<1$, corresponds to the unphysical domain. We define another function $g(\omega,t)$, which is the derivative of the function f with respect to ω,

$$g(\omega,t)=\frac{\partial f(\omega,t)}{\partial\omega} \ . \tag{5}$$

To make the solution meaningful, all the zeros and poles of g have to remain inside the unit circle. Using this formulation and rescaling the variables in the problem, we can reduce the above equations into one equation describing the time evolution of the mapping function $f(\omega,t)$,

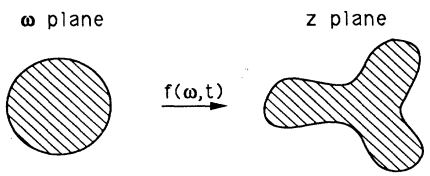

FIG. 2. The mapping. A conformal map $f(\omega,t)$ maps a unit circle in the ω plane onto the real physical interface and the outside of the circle into the outside of the bubble. The outside of the unit circle is the physical domain and the inside is the unphysical domain where the singularities lie.

$$\frac{\partial f}{\partial t}=\omega\frac{\partial f}{\partial\omega}\hat{A}\left\{\frac{1-d_0\mathrm{Re}(\omega\partial/\partial\omega\,\hat{A}\{\kappa\})}{|\partial/\partial\omega f|^2}\right\}, \tag{6}$$

and the corresponding equation for g is

$$\frac{\partial g}{\partial t}=\frac{\partial}{\partial\omega}\left[\omega g\hat{A}\left\{\frac{1-d_0\mathrm{Re}(\omega\partial/\partial\omega\,\hat{A}\{\omega\})}{|g|^2}\right\}\right] . \tag{7}$$

This equation describes the situation in which the area of the bubble grows linearly with time. Specifically, the time derivative of the area is 2π. In Eqs. (6) and (7), $\hat{A}$ is an operator that acts on functions that are analytic in an annular region containing the unit circle. For a function $F(\omega)$ that can be expressed, in the neighborhood of the circle, as

$$F(\omega)=\sum_{n=-\infty}^{\infty}a_n\omega^n \ , \tag{8}$$

we define

$$\hat{A}\{F(\omega)\}=a_0+2\sum_{n\ (\leq -1)}a_n\omega^n \ . \tag{9}$$

The curvature κ can be expressed in terms of $f(\omega,t)$ as

$$\kappa=-\mathrm{Re}\left[\frac{\partial/\partial\omega f+\omega\partial^2/\partial\omega^2 f}{\partial/\partial\omega f\,|\partial/\partial\omega f|}\right] . \tag{10}$$

Equation (7) contains a parameter d_0 that is proportional to the surface tension in the system. d_0 has the dimension of a length and it can be expressed, in terms of the parameters of the system, as

$$d_0=\frac{\pi^2\tau b^2}{3\mu dS/dt} \ , \tag{11}$$

where dS/dt is the time derivative of the area of the bubble. In our numerical work below, we set dS/dt equal to 2π. The initial value of the zeroth Fourier coefficient of the function g, $A(0)$, which has the dimension of a length, is set equal to 1 in order to give a length scale to the system and thus to make d_0 dimensionless.[11]

Following the work in Refs. 8, 2, and 5, we use the singularities in the unphysical domain to describe the analytic structure of the function g and some physical quantities of the bubble. We know that this method works when the surface tension is zero, and hope that the study of the singularities can give an effective treatment of the problem when the surface tension is not zero.

III. BRIEF REVIEW OF THE ZERO-SURFACE-TENSION CASE

Before moving on to the simulation results for the on zero-surface-tension case, we give a brief review of some previous work on the bubble growth at zero surface tension.[2,3,5,8] We choose our initial condition for $g(\omega,t)$ to have the zero or (and) pole structure:

$$g(\omega,t)=A(t)\frac{\prod_{i=1}^{m}(1-z_i(t)/\omega^q)}{\prod_{j=1}^{n}(1-p_j(t)/\omega^q)} \ , \tag{12}$$

where $A(t)$ is real. For $m \geq n$,[12] this analytic structure will be preserved, and the original partial differential equation is reduced to some ordinary differential equations governing the evolution of the zeros $z_i(t)$, the poles $p_j(t)$, and the number $A(t)$, which is the dc component of the Fourier spectrum of the function g.

For zero surface tension, the work of Sarkar and Jensen[5] has given a good description of what happens when all the singularities of g are, in fact, zeros. Then it is almost always true that one or more of the zeros will hit the unit circle. At that critical time, the interface will usually develop cusps, and the solution will break down.

A particular simple situation arises when we have q zeros symmetrically placed within the unit circle. In this q-zero case, the solution has the structure

$$g(\omega,t)=A(t)\left[1-\frac{z(t)}{\omega^q}\right] . \tag{13}$$

Without loss of generality, we can take $z(t)$ to be real.

The equations of motion for $A(t)$ and $z(t)$ are

$$\frac{dA}{dt}=\frac{1}{A(t)[1-z^2(t)]} , \tag{14}$$

$$\frac{dz(t)}{dt}=\frac{(q-2)z(t)}{A^2(t)[1-z^2(t)]} . \tag{15}$$

For $q=3$, they have the solutions

$$A(t)=\frac{A(0)}{z(0)}\left[1-\left[1-2z^2(0)+z^4(0)-4t\frac{z^2(0)}{A^2(0)}\right]^{1/2}\right]^{1/2} , \tag{16}$$

$$z(t)=\frac{z(0)}{A(0)}A(t) , \tag{17}$$

where $A(0)$ and $z(0)$ define the initial conditions. Notice that when t reaches the critical time t_c,

$$t_c=\left[\frac{A(0)[1-z^2(0)]}{2z(0)}\right]^2 , \tag{18}$$

where $z(t_c)$ is one and the solution becomes singular. The equations and the solutions then fail to make sense for $t>t_c$. This t_c is the critical time we mentioned at the start.

In Fig. 3, interfaces are shown at $t=0$, 0.18, 0.36, and 0.54 for the q-zero case with $q=3$, $A(0)=1.0$, and $z(0)=0.5$. The tips of the interface get sharper at later times, and they will develop into cusps at the critical time, which, according to Eq. (18), is about 0.5625.

In contrast, we can consider cases in which the solution remains valid for all times.[3] The simplest of these is the case that we call the q-pole case. Here there are q poles and q zeros, but the poles remain closer to the unit circle than the zeros. The solution has the following structure:

$$g(\omega,t)=A(t)\frac{1-z(t)/\omega^q}{1-p(t)/\omega^q} , \tag{19}$$

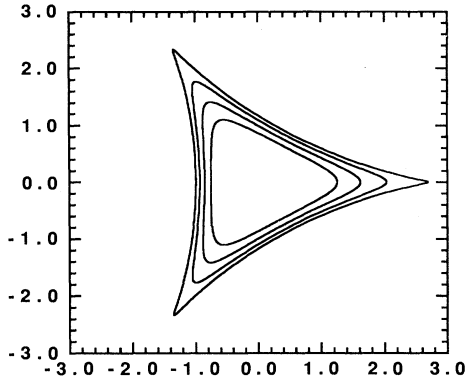

FIG. 3. Evolution of a bubble with $d_0=0$ for the q zero case. The corresponding times for the interfaces from inside out are 0.00, 0.18, 0.36, and 0.54.

where $z(t)$ and $p(t)$ describe, respectively, the positions of the zeros and the poles. We shall consider only the case when A, z, and p are real and obey $0<z(0)<p(0)<1$. Then the solution will be one in which the poles and the zeros move asymptotically toward the unit circle but never get there. Furthermore, for $t>0$, we have $z(t)<p(t)<1$, so the solution exists for all times. For very large times, the asymptotic solution is

$$A(t)=(2t)^{1/2} , \tag{20}$$

$$p(t)=1-c_2\exp\left[-q\frac{t^{1/2}}{c_1}\right] , \tag{21}$$

$$z(t)=1-\frac{c_1}{t^{1/2}} , \tag{22}$$

where c_1 and c_2 are two constants of integration.

In Fig. 4, interfaces with three-fold symmetry at times 0, 5, 10, 15, and 20 are shown. The initial condition is $A(0)=1.0$, $p(0)=0.5$, $z(0)=0.0$. Fjords, channels of the viscous fluid (fluid 2) where the growth of the bubble

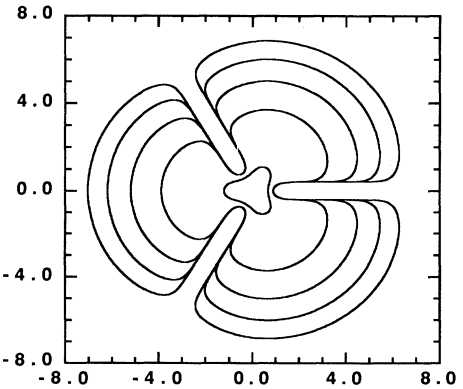

FIG. 4. Evolution of a bubble for $d_0=0$ with threefold symmetry and the q-pole initial conditions. The times shown are 0, 5, 10, 15, and 20.

is greatly suppressed, develop at later times. In this case, the fjords are almost perpendicular to the fronts that almost form a circle. This reflects the fact expressed in Eqs. (21) and (22) that the poles and the zeros tend to 1, but the poles approach much faster then the zeros do.

IV. SIMULATION RESULTS FOR THE NONZERO-SURFACE-TENSION CASE

In our simulations, we consider in detail two cases that have initial conditions of the q-zero and the q-pole cases described above.

A. Pole initial condition

1. Smaller surface tension

For the analog of the q-pole case for zero surface tension, we used $d_0=10^{-3}$, and took as the initial condition

$$g(\omega,t)|_{t=0}=\frac{1}{1-0.5/\omega^3} . \tag{23}$$

In our previous notation, $A(0)=1.0$, $z(0)=0.0$, $p(0)=0.5$, $q=3$.

Figure 5 is the interface up to time $=0.6$ for $d_0=10^{-3}$. For times no later than 0.6, the interfaces are almost identical to those with $d_0=0$. We are not able to carry the calculation for the nonzero-surface-tension case long enough to see if the interesting shape exhibited by the zero-surface-tension case shown in Fig. 4 will show up when the surface tension is not zero.

Since g_n, the nth Fourier coefficient of the function g, is also the coefficient of the term ω^{-nq} in the Taylor expansion (see the Appendix), the dependence of g_n on n gives information on the analytic structure of the function g. Whenever the singularity nearest the unit circle is a branch cut of order γ that lies at $\omega^q=p$, the leading behavior of the ratio of the coefficients is

$$|g_{n+1}/g_n| \underset{n\to\infty}{\sim} |p|\left[1-\frac{1+\gamma}{n}\right] .$$

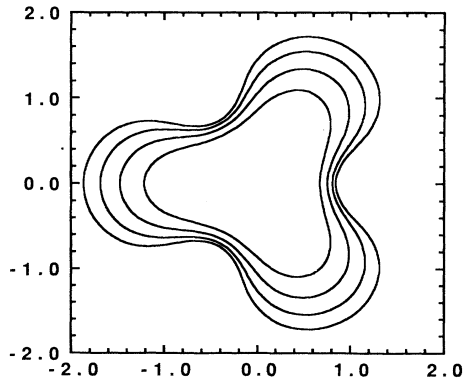

FIG. 5. Evolution of a bubble for $d_0=10^{-3}$ with threefold symmetry and the same initial condition as in Fig. 4. The times for the interfaces shown are 0.0, 0.2, 0.4, and 0.6. The shape of the interface up to $t=0.6$ is almost identical to that without surface tension.

Especially, if the leading singularity is pole singularity, $\gamma=-1$, the above ratio goes like $|p|$ and the coefficients

$$g_n \underset{n\to\infty}{\sim} |p|^n .$$

Figure 6(a) shows the Fourier coefficients g_n generated by the simulation at time $=0.6$. The almost-linear behavior of this log-linear plot shows that the singularity is pole-like, but the highest frequencies do show some deviation from a straight line. By measuring the slope of the curve on this log-linear plot, we can find the quantity $p(t)$, the qth power of the distance between the leading singularities and the center of the unit circle. This quantity is plotted against time t in Fig. 7. In Fig. 6(b), g_{n+1}/g_n is plotted against $1/n$ for time $=0.6$. This ratio is almost a constant, but it does show a small but important variation. This variation indicates that the singularity structure is not simply described by a single quantity $p(t)$ that describes the positions of the poles. By extrapolating the ratio $g_{n+1}g_n$ to $n\to\infty$, or $1/n\to 0$, we can also get $p(t)$ from the following:

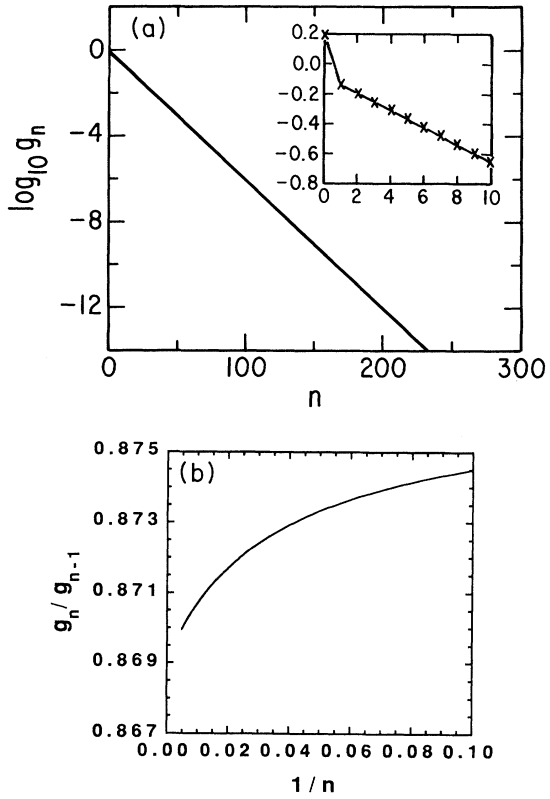

FIG. 6. Behavior of expansion coefficients for the largest bubble shown in Fig. 5. (a) The Fourier coefficients g_n in logarithmic scale. The almost-exponential behavior suggests a pole-like singularity structure for the function g. The inset gives the first ten Fourier coefficients in logarithmic scale. (b) g_{n+1}/g_n vs $1/n$. The nonlinear behavior indicates that a single quantity describing pole or branch-cut structure cannot describe all of the singularity structure of the function g. But the extrapolation of the curve to $1/n\to 0$ tells us roughly where the leading singularity is.

$$p(t) \underset{n\to\infty}{\sim} \frac{g_{n+1}}{g_n} .$$

The values of $p(t)$ obtained from these two methods differ by 1 part in 10^3.

In Fig. 7, where $p(t)$'s for both cases were plotted, we can see some small changes caused by the surface tension. Notice that the singularity moves more slowly towards the unit circle when surface tension is present than when the surface tension is zero, and that in both cases the singularities approach the unit circle as time goes to infinity.

We also studied a bubble with fourfold symmetry, since other workers have considered this case in some detail.[13] Behavior in the shape of the interface and the movement of the singularities was found to be similar for $d_0=10^{-3}$ to that for the previous case with threefold symmetry. The initial condition was

$$g(\omega,t)|_{t=0}=\frac{1}{1-\frac{0.1}{\omega^4}} . \tag{24}$$

The interfaces at $t=0$, 0.5, 1, and 2 are shown with those of $d_0=0$ in Fig. 8(a), and the corresponding movements of the leading singularities are shown in Fig. 8(b). Again, we see a behavior in the Fourier coefficients that indicates that the analytic structure of g up to that time can be described by a polelike singularity, similar to the zero-surface-tension case. But there is some visible difference for larger times in the shape of the interface at the places where fjords develop in the zero-surface-tension case. This difference might be important for determining the singularity structure of the function g. Following Thome *et al.*,[13] a ratio λ, similar to that in the Saffman-Taylor finger problem,[6] which is the ratio of the finger to the width of the channel, can be defined. We can look at the interface as one that is composed of q parts, each part identical (assuming we only consider the case where the singularities are real). Since there is no flow between each part according to the symmetry, the properties of each part are the same as those of the fluid restrained between two intersecting walls that intersect at the injection point with an angle of $2\pi/q$. Hakim *et al.* found experimentally that in a situation with two walls, the interface will grow steadily after some time and form a fingerlike structure that has a characteristic angle. The ratio of this angle to the angle between the walls is defined to be λ. If the growth of the interface really follows that of the zero-surface-tension case seen in Fig. 4, λ goes to 1 as time goes to infinity, which disagrees both with a theoretical result of λ obtained by Brener *et al.*[14] and an experimental result by Arneodo *et al.* for a case with fourfold symmetry.[15] From Fig. 8(a), one cannot tell whether the interface will form a finger with some asymptotic value of λ or what the value of λ might be.

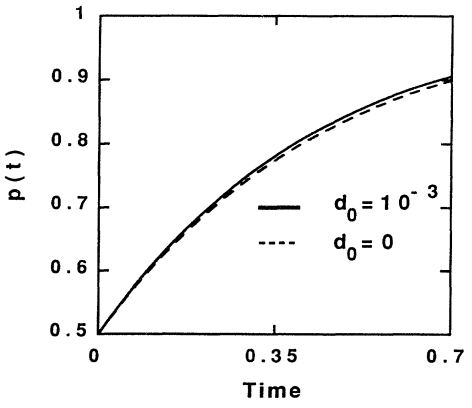

FIG. 7. The motion of the leading singularity for the simulations shown in Figs. 4 and 6. Here $p(t)$ is plotted against time for $d_0=10^{-3}$ (solid line) and $d_0=0$ (dotted line).

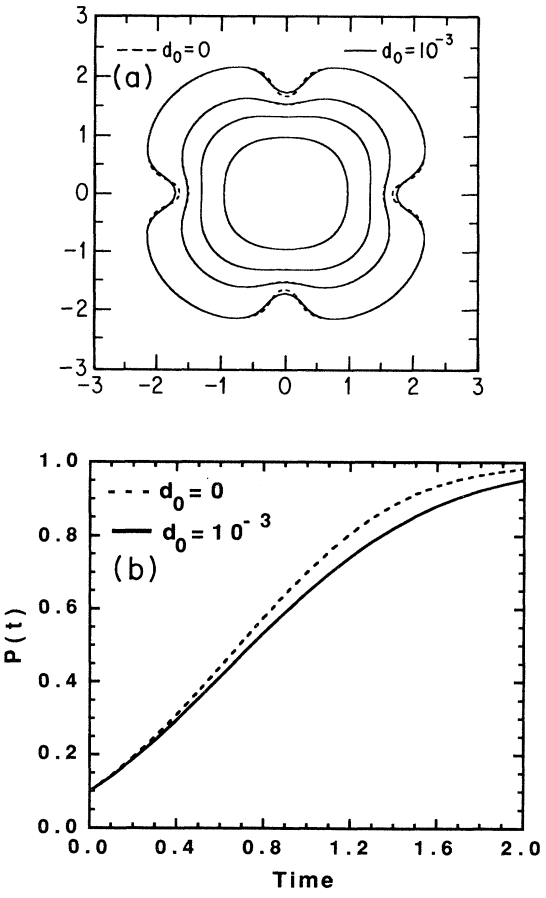

FIG. 8. The interfaces for fourfold symmetry. The comparison for the shape of the interface (a) and the motion of the singularities (b) between $d_0=10^{-3}$ (solid lines) and $d_0=0$ (dotted lines) for an initial q-pole case. In both cases, the interface has a fourfold symmetry and the initial condition is $A(0)=1.0$, $z(0)=0.00$, $p(0)=0.1$. (a) The corresponding times are 0.0, 0.5, 1.0, and 2.0 from inside out. The evolution of the interface with nonzero surface tension follows that without surface tension closely. But we do see some difference at the latest time at the places where fjords develop when there is no surface tension. (b) We see again as in Fig. 7 that the motion of the polelike singularities towards the unit circle is slowed down by the surface tension.

2. Larger surface tension

We used again the same initial condition as in (23), but chose $d_0=10^{-1}$. Figure 9(a) shows the interfaces as times 0, 0.5, 1, and 1.5. Figure 9(b) shows the interfaces for $d_0=0$ at the same times as those in Fig. 9(a). The surface tension changes the interfaces considerably. With zero surface tension, the interface at $t=1.5$ has already started to develop fjords; while with this relatively large surface tension, the interface becomes circular as time goes on. The structure of the Fourier spectrum does not change much, but the motion of the singularities is towards the center of the unit circle instead of towards the unit circle. Figure 10 shows $p(t)$, which describes the motion of the leading singularities with respect to time with and without surface tension. Notice that in the presence of surface tension, the leading singularities move towards the center of the unit circle. This motion makes the actual interface become rounder and rounder.

The linear analysis gives us some idea as to why this happens. The rate of change for the nth Fourier coefficient is proportional to $qn-d_0n^3q^3$. When the surface tension is of the order of $1/q^2$, this rate of change becomes negative even for $n=1$. Indeed, for $q=3$, we found that the behavior of the singularity changes when the surface tension is of the order of 0.1.

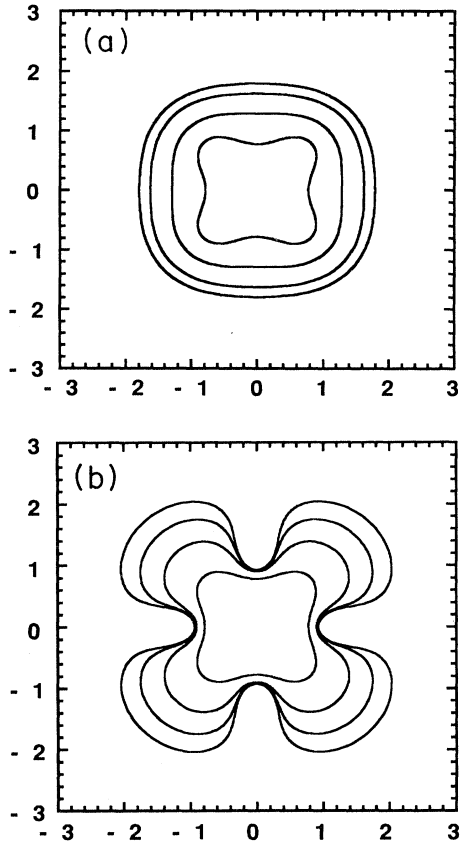

FIG. 9. Interface motion with larger d_0. The q-pole initial condition used is the same as that in Fig. 8. The times are 0, 0.5, 1, and 1.5. The interface in (a) has $d_0=10^{-1}$, while the one in (b) has $d_0=0$. As in Fig. 4, fjords develop against an almost circular front when there is no surface tension. But when there is relatively larger surface tension, the interface gets more and more like a circle, which is a result of the polelike singularities moving towards the center of the unit circle, as is shown in Fig. 10(b).

B. Initial condition of the q-zero form

1. Smaller surface tension

To find the finite-surface-tension analog of the q-zero behavior, we first used $d_0=10^{-3}$, and the initial condition

$$g(\omega,t)|_{t=0}=1-\frac{0.5}{\omega^3} . \tag{25}$$

Thus, in the previous notation, $A(0)=1.0$, $z(0)=0.5$, $q=3$.

Figure 11(a) shows the resulting interfaces for $d_0=10^{-3}$ at $t=0$, 0.18, 0.36, 0.54, and 0.59. Here the critical time when $d_0=0$ is $t_c=0.5625\ldots$. We can see that for the $d_0=0$ case (Fig. 3), the tips of the interface develop into cusps when $t=t_c$, while for $d_0=10^{-3}$, the tips look much rounder. In the latter case, we can carry the calculation beyond t_c. In Fig. 11(b), the two cases are compared for $t<t_c$.

From the two dents in the sides of the finite-surface-tension interface [see Fig. 11(b)], one might guess that $g(\omega,t)$ perhaps has two identical singularities, complex conjugates of one another. If these are the singularities that lie closest to the unit circle and lie at $p(t)$ and $p^*(t)$, which, respectively, has phases $+\theta(t)$ and $-\theta(t)$, then for large n, the Fourier coefficient will have the following form:

$$g_n=C_n|p(t)|^n\cos(n\theta) , \tag{26}$$

where C_n changes very slowly in comparison with the other two quantities.

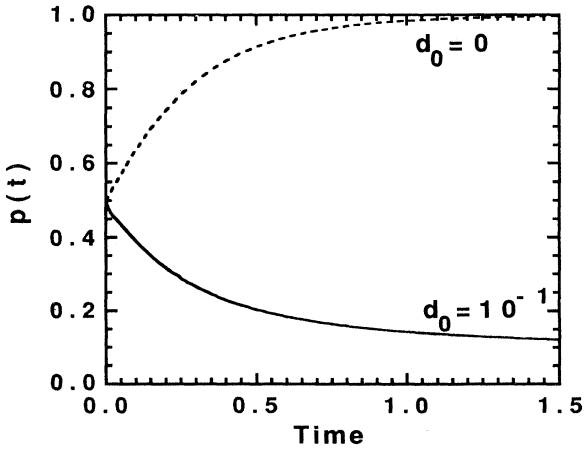

FIG. 10. The motion of singularities for the flows shown in Fig. 9.

The actual Fourier coefficients g_n, as shown in Fig. 12(a), has an n dependence rather similar to (26). We fit the envelope to the data by a straight line to get an estimate of $|p|$. The we apply Fourier transform to the series $g_n e^{n|p|}$ to get an estimate of θ. Finally, we change $|p|$, θ, and θ_0 around their estimated values to get the best fit. If the structure in Eq. (26) is true, the quantity $R_n = g_n/(e^{|p'|}g_{n+1} + e^{-|p'|}g_{n-1})$ should be weakly dependent on n. Furthermore, as $n \to \infty$, this ratio goes to $2/\cos(\theta)$ when $|p'| = |p|$. In Fig. 12(b), where R_n is plotted against n, we see that for the high frequencies, R_n does become constant. The positions of the singularities fit by the two different methods agree to 1%. Given fits of this quality, it seems reasonable to call $p(t)$ and $p^*(t)$ the positions of the singularities.

Figure 13 shows how these singularities move inside the unit circle. Here we are looking at the singularities in the ω plane. The original three zeros are marked by Δ in the figure. Each of them splits into two poles, which then move towards the unit circle. Figure 14(a) shows how the quantity $1-|p(t)|$, a measure of the distance between the singularities and the unit circle, changes as a function of time. The distance is plotted on a logarithmic scale. It suggests that the singularities might approach the unit circle exponentially in time. Figure 14(b) shows the phase of $p(t)$ as a function of time.

These singularities may not be poles. The basic equations do not seem to admit pole solutions,[16] but nonetheless the singularities generated by the numerical work do appear isolated and polelike.

We then did a calculation for a case with sixfold sym-

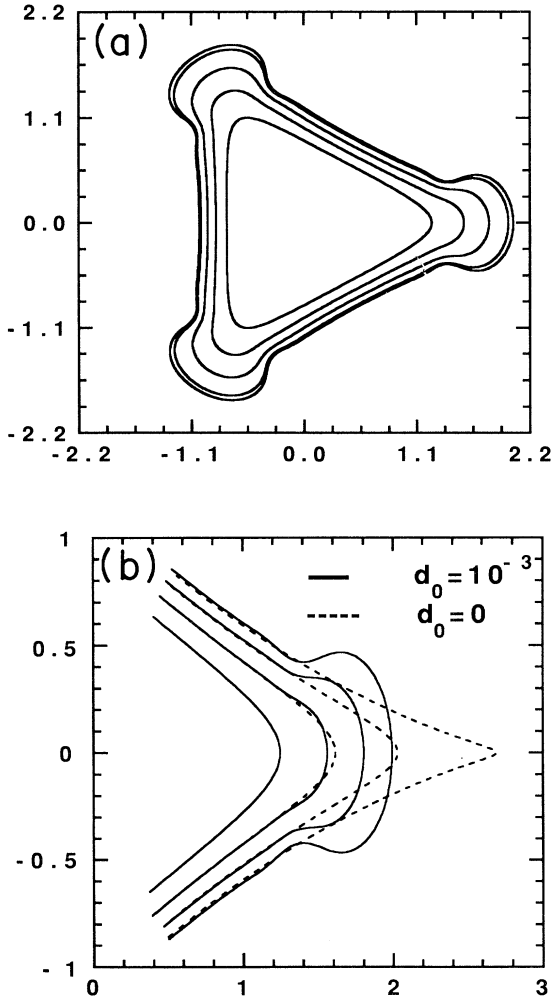

FIG. 11. The three-zero initial condition is run with finite surface tension. The initial condition is the same as that in Fig. 3. The innermost bubble is our initial condition; the times for the other bubbles are 1.18, 0.36, 0.54, and 0.59 from inside out. (a) The interface development. (b) Figure 3 (dotted lines) and (a) (solid lines) are compared. Only one third of the interface is shown here.

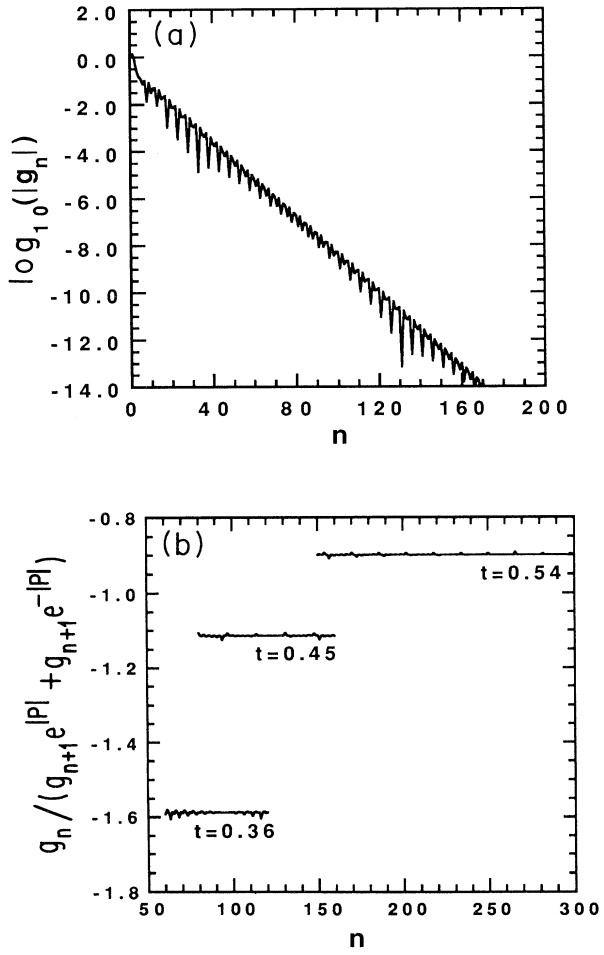

FIG. 12. Plot of g_n vs n for the case depicted in Fig. 11. (a) Plot of $\log_{10} g_n$ vs n at time $=0.36$. The periodic bumps on top of a straight line suggests a two-pole-like singularity structure for each of the three parts of the interface. (b) $g_n(e^{|p'|}g_{n+1} + e^{-|p'|}g_{n-1})$ is plotted against n for high frequencies for times 0.36, 0.45, and 0.54, corresponding to the bubbles shown in Fig. 11(a). The almost-horizontal lines confirm the previous observation that the leading singularity structure is two-pole-like for each of the three parts of the interface.

metry and an even smaller surface tension $d_0=10^{-4}$. The initial condition was

$$g(\omega,t)|_{t=0}=1-\frac{0.1}{\omega^6} . \tag{27}$$

We found similar behavior in both the shape of the interface and the motion of the singularities. Figure 15(a) shows the interfaces at different times compared with those of $d_0=0$. The critical time for zero surface tension is 0.7659. . . . Again, with small surface tension, we could calculate the interface beyond that time. Figure 15(b) shows the motion of the singularities in the complex plane. In this case, each of the six points in the complex plane (which correspond to the sixth roots of the initial zero) splits into a pair of poles that are complex conjugates to each other, and the resulting poles move towards the unit circle.

2. *Larger surface tension*

For relatively large surface tension, we found different behavior of the singularities. Consider the surface tension 10^{-2} and the initial condition

$$g(\omega,t)|_{t=0}=1-\frac{0.1}{\omega^4} . \tag{28}$$

When $t>0$, the Fourier coefficients alternate in their signs, and the logarithm of the absolute values of the g_n's shows a linear relationship with n (see Fig. 16), and the slope of the line increases with time. This means that the leading singularities are polelike and are described by a quantity $p(t)$. This quantity lies on the opposite side of the real axis from the quantity $z(0)$ that describes the initial zero and moves towards -1. We can understand the change of the nature of the singularity in the following fashion. Consider a function of the form $1/(1+0.1/\omega^4)$, whose pole singularities are described by the quantity -0.1; it can be expanded into, ignoring the higher-order terms, $1-(0.1/\omega^4)$, whose zero singularities are described by the quantity $+0.1$. So ignoring the higher-order terms, a q-zero initial condition could be considered as almost a q-pole case, with the kth pole of the total q poles having an extra phase factor of $(k-1)\pi/q$. We think that under relatively larger surface tension, the polelike singularities, described by a quantity $p(t)$, which lies on the different side of the real axis from the quantity $z(0)$, which describes the initial zeros, might have come from this "almost q-pole" initial condition.

The interfaces at different times are shown with those of $d_0=0$ in Fig. 17. We have carried the calculation much longer than the critical time for zero surface ten-

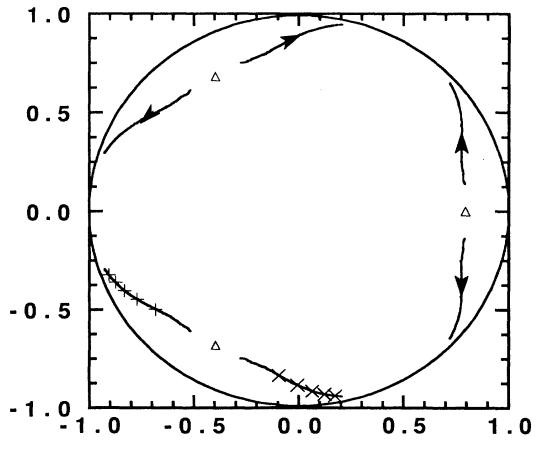

FIG. 13. Motion of singularities for the case shown in Figs. 11(a) and 12. The loci of the singularities are shown inside the unit circle. The initial zeros which are cubic roots of 0.5 are denoted by △. Each of them splits into two poles, which are complex conjugates to each other, and the resulting poles move towards the unit circle. On the bottom lines, towards the unit circle, the symbols × mark the position of the poles on those two lines for times 0.1, 0.2, 0.3, 0.4, and 0.5.

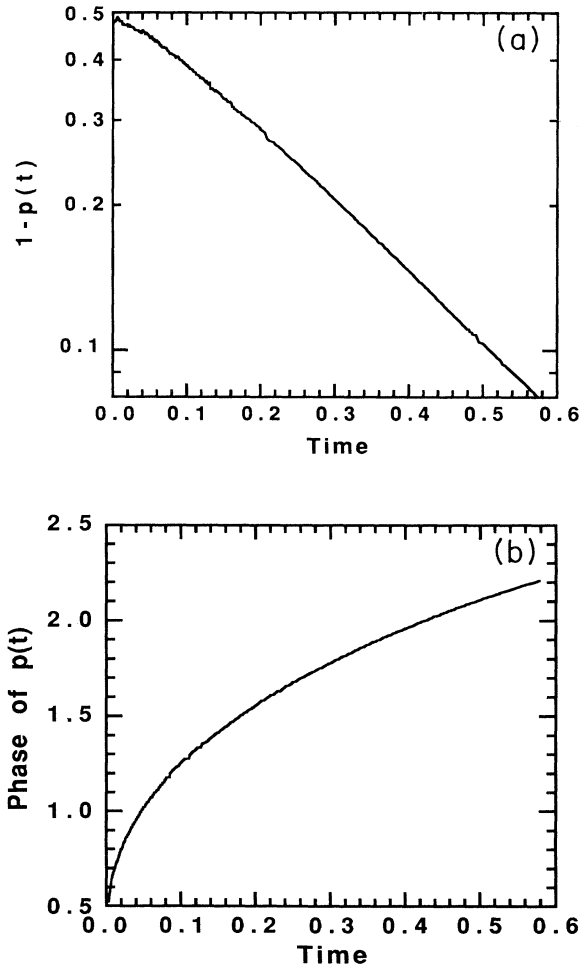

FIG. 14. Position of the singularities for the case shown in Fig. 13(a). $1-p(t)$, the measure of distance between the singularities and the unit circle from our fitting results, is plotted in logarithmic scale against time. It looks like a straight line for large time, which suggests that the poles might asymptote the unit circle exponentially in time. (b) The phase of $p(t)$ in rad vs time.

sion, which is 2.8349. . . .

We also found, for some intermediate values of surface tension, some intermediate behavior between what we found for relatively small and relatively large surface tension. For some early times, the logarithm of the absolute values of the Fourier coefficients versus frequencies had some bumps on top of a straight line, which was similar to the behavior found when relatively small surface tension was used, as in Fig. 12, except that the number of bumps was much smaller and decreased with time. After some time interval, the bumps disappeared, and we saw the same behavior as we did when relatively large surface tension was used, as in Fig. 16. We have not studied this behavior sufficiently to fully understand it. We speculate that the reason for this to happen might be the following. Initially, as in the case with relatively small surface tension, each initial zero turned into two poles that were complex conjugates to each other except that they lay on the other half of the complex plane, and then the two poles merged into one and moved towards -1.

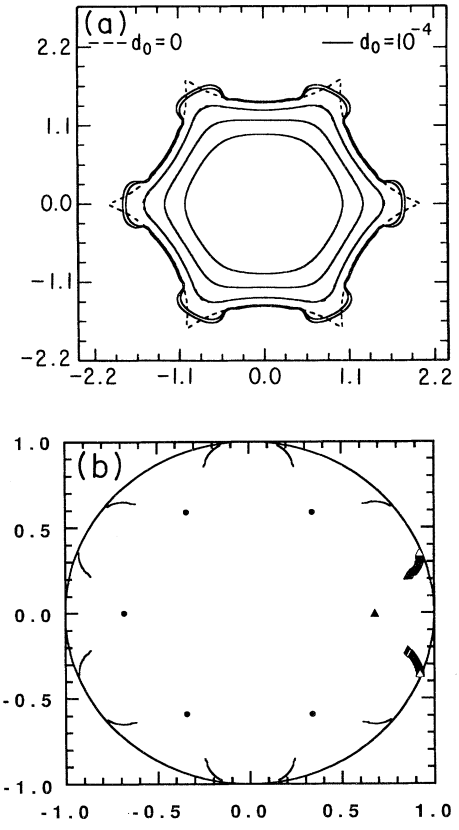

FIG. 15. Motion of an interface that has sixfold symmetry. The q-zero initial condition used is $A(0)=1.0$, $p(0)=0.0$, $z(0)=0.1$. (a) The evolution of a bubble with and without surface tension. The zero-surface-tension case is shown as the dotted lines for $t=0.0$, 0.25, 0.50, and 0.75. The bubbles with $d_0=10^{-4}$ are shown as the solid lines for $t=0.0$, 0.25, 0.50, 0.75, and 0.80. The bubble without surface tension develops cusps around $t=0.77$. Again, we were able to calculate the problem beyond that time with even small surface tension. (b) The motion of the singularities inside the unit circle for $d_0=10^{-4}$. The initial zeros, which are sixth roots of 0.1, are marked by dots, except that the one on the real axis is marked by ▲, and the resulting polelike singularities of this point in later times are marked by △. As in Fig. 13, each of the initial zero splits into two polelike singularities, which are complex conjugates to each other and move towards the unit circle.

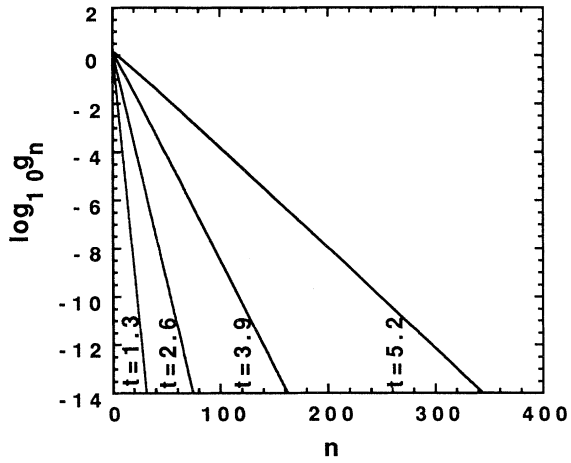

Fig. 16. $\log_{10} g_n$ vs n for an initial q-zero case with a larger surface tension (10^{-2}) and the same initial condition as that in Fig. 15(a). The straight line suggests that the singularity is a polelike, which is different from what is shown in Fig. 12(a). The corresponding times are 1.3, 2.6, 3.9, and 5.2. Since the slope of the lines increases with time, the polelike singularities move towards the unit circle.

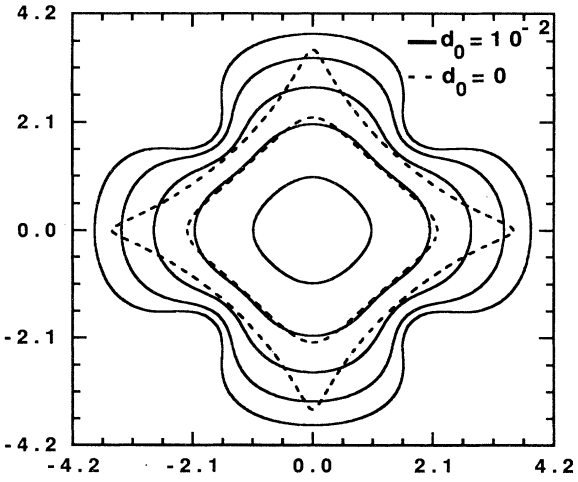

FIG. 17. The growth of a bubble without surface tension (dashed lines) and with surface tension 10^{-2} (solid lines) with the same initial conditions as those in Fig. 16. The times for the zero-surface-tension case are 0, 1.3, and 2.6; for the nonzero-surface-tension case, 0, 1.3, 2.6, 3.9, and 5.2. The critical time is roughly 2.83. Again, with nonzero surface tension, we could carry the calculation long after the critical time.

V. CONCLUSIONS

We calculated the bubble growth in the Hele-Shaw cell for the nonzero-surface-tension case and compared them with the corresponding zero-surface-tension case. For the q-zero initial condition, a small surface tension does change the shape of the interface significantly, and the existence of this small surface tension enables us to carry our calculation longer than the critical time. But for the q-pole initial condition, a small surface tension does not seem to affect the solution very much. In all the cases considered, a relatively large surface tension changes the solution qualitatively considering both the shape of the interface and the motion of the singularities. We notice that polelike singularities seem to maintain this form even with nonzero surface tension. Conversely, an initial condition with zeros in g is quite unstable against the "perturbation" caused by surface tension. We speculate that isolated singularity structures might be a good solution to the equations even for nonzero surface tension, and that these singularities might maintain their form even at very large time, when the singularity position asymptotically approaches the unit circle.

Note added in proof. After we submitted the manuscript, we did some more studies on the initial q-zero case with a small surface tension. It seems that the analytic structure of the function g can perhaps be better described by a continuous distribution of polelike (more precisely, branch cuts of some power) structures and their complex conjugate on a circle with a radius smaller than 1. We suspect that this might also be the case for the initial q-pole case. Further studies are needed to determine the nature and the number of these singularities.

ACKNOWLEDGMENTS

The authors would like to thank the following people for helpful discussions: P. Constantin, A. Libchaber, B. Shaw, M. Shelley, and S. Tanveer. This work is supported by the Office of Naval Research (ONR) and the University of Chicago Materials Research Laboratory. We would also like to acknowledge the support of Cornell National Supercomputer Facility (CNSF) and National Center for Supercomputer Applications (NCSA) at Urbana-Champaign for computational facilities.

APPENDIX: COMPUTATIONAL METHODOLOGY

Following Bensimon,[8] we use a pseudospectral method to solve Eq. (7). We can make a Fourier expansion of the function $g(\omega,t)$, which is also its power expansion in ω, since ω is on the unit circle. Considering the q-fold symmetry on the unit circle in the ω plane, this expansion looks like

$$g(\omega,t)=\sum_{n=0}^{\infty} g_n(t)\omega^{-nq} . \tag{A1}$$

The expansion is truncated at a certain number of terms N, beyond which all g_n fall into roundoff error. All the space derivative calculations are carried out in the Fourier space and then transformed back to the real physical space if necessary. The analytic continuation is done in the Fourier space using Eq. (9). In order to better control the growth of the high frequencies, we add and subtract a linear damping term, which we get from linear analysis, to the time derivative of the Fourier coefficients. So the equations in the Fourier space look like

$$\frac{dg_n}{dt}=L_n g_n+(N_n-L_n g_n) , \tag{A2}$$

where N_n is the nth Fourier coefficient of the right-hand side of Eq. (7) and L_n from linear analysis, is proportional to $qn-d_0 n^3 q^3$. For high frequencies, i.e., large n, L_n is negative. Equation (A2) is then solved using a method similar to the second-order Runge-Kutta method. In the simulation, we incorporate the q-fold symmetry into our scheme to save time. In most of the cases considered, as t increased, the singularities moved towards the unit circle and the high Fourier coefficients grew steadily. When the highest frequency components exceed the roundoff error, the errors in the highest Fourier frequencies will propagate to the lower ones until the solution diverges. To make the solution converge, we had to use more frequency components in the calculation so that the highest frequency components were always smaller than the roundoff error. Since we used fast Fourier transform routine to do the Fourier transform, we doubled the number of points and give them an initial value of zero just before the highest frequency components exceeded the round-off error.

In the calculation where $d_0=10^{-3}$ and a q-pole initial condition was used, we began with the first 256 terms of the Fourier transform of the function g (half of which were of the negative frequencies and were therefore nonzero), and the corresponding time step was 10^{-6}. Before the highest Fourier component exceeded the roundoff error, we doubled the number of points by assigning the rest to be zero and decreased the time step accordingly. Generally, if the number of points used is N, the time step used is proportional to d_0/qN^3. We stopped the calculation just before the highest frequency of the Fourier spectrum of 1024 points exceeded the roundoff error, the time step being 10^{-7}. In order to check the program, we did another calculation for the same problem. We began with 1024 points and a time step of 10^{-7}. After 3 000 000 iterations (when the time was 0.3), we compared the Fourier components with those obtained from the previous calculation. The lower Fourier coefficients agreed to the tenth or eleventh digit, and the higher Fourier coefficients agreed to the twelfth or thirteenth digit.

[1]For bubble growth, see, for example, L. Paterson, J. Fluid Mech. **113**, 513 (1981); Phys. Fluids **28**, 26 (1985); S. N. Rauseo, P. D. Barnes, Jr., and J. V. Maher, Phys. Rev. A **35**, 2840 (1987). For Hele-Shaw finger growth, see, for example, T. Maxworthy, Phys. Rev. A **39**, 5863 (1989), and the references cited in Ref. 7.

[2]B. Shraiman and D. Bensimon, Phys. Rev. A **30**, 2840 (1984).

[3]S. D. Howison, J. Fluid Mech. **167**, 439 (1986).

[4]D. Bensimon and P. Pelce, Phys. Rev. A **33**, 4477 (1986).

[5]S. Sarkar and M. Jensen, Phys. Rev. A **35**, 1877 (1987).

[6]P. G. Saffman and G. I. Taylor, Proc. R. Soc. London, Ser. A **245**, 312 (1958).

[7]*Dynamics of Curved Fronts,* edited by P. Pelce (Academic, San Diego, 1988), and references cited therein.

[8]D. Bensimon, L. P. Kadanoff, S. Liang, B. I. Shrainman, and C. Tang, Rev. Mod. Phys. **58**, 977 (1986).

[9]S. Tanveer, Phys. Fluids **30**, 1589 (1987), and unpublished.

[10]See, for example, C. -W. Park and G. M. Homsy, J. Fluid Mech. **139**, 291 (1984); J. W. Maclean and P. G. Saffman, *ibid.* **102**, 455 (1981).

[11]In the situation of a channel flow, a dimensionless capillary number similar to $1/d_0 L$, Ca, can be defined, where L is the width of the channel. Following Meiberg and Homsy, [E. Meiberg and G. M. Homsy, Phys. Fluids **31**, 429 (1988)]. $\mathrm{Ca}=3\mu u L^2/\tau b^2$, where u is the mean velocity with which fluid 1 is injected. So uL in the channel is the area growth rate dS/dt in the bubble-growth case. If we take L to be 2π as per Meiberg and Homsy the value of dimensionless d_0 is the value of π^2/Ca and correspondingly, the value of the product of $4\pi^2$ and the dimensionless surface tension in the calculation of Tryggvason and Aref [G. Tryggvason and H. Aref, J. Fluid Mech. **136**, 1 (1983); **154**, 287 (1985)] and Degregoria and Schwartz [A. J. Degregoria and L. W. Schwartz, Phys. Rev. Lett. **58**, 1742 (1987)].

[12]If $m < n$ initially, there will be $n - m$ extra zeros when $t > 0$.

[13]H. Thome, M. Rabaud, V. Hakim, and Y. Couder, Phys. Fluids A **1**, 224 (1989).

[14]E. A. Brener, D. A. Kessler, H. Levine, and W. Rappel, Europhys. Lett. **13** (2), 161 (1990).

[15]A. Arneodo, Y. Couder, G. Grasseau, V. Hakim, and M. Rabaud, Phys. Rev. Lett. **63**, 984 (1989).

[16]L. P. Kadanoff, Phys. Rev. Lett. **65**, 2986 (1990).